Multi-spectral Shocklayer Radiance from a Hypersonic Slender Body

Deborah A. Levin*
George Washington University,
Washington, DC 20052

David M. Mann†
Army Research Office
Research Triangle Park, NC 27709-2211

Clifton B. Phillips‡
Mike Lovern
SPAWAR Systems Center
San Diego, CA 92152-5070

Carl Howlett§
Space Dynamics Laboratory
Utah State University
Logan, UT 84322-4140

Peter Erdman¶
Embry-Riddle University
Daytona Beach, FL, 32114

Abstract

The Science and Technology Directorate of the Ballistic Missile Defense Organization is conducting programs to characterize and measure the radiation emitted by the flows about hypersonic vehicles. In addition to understanding the basic physics of high temperature plasmas, ongoing analyses are establishing how such emissions are useful for the detection of theater missile targets using the mid-wave infra-red (MWIR) spectral region (3 - 5 μ) as the baseline and the ultraviolet (UV) or visible wavelengths as a second detection wavelength.[1] The use of a second, shorter wavelength combined with the baseline sensor increases the total information content of the scene. This paper will present a methodology for the calculation of the self-induced, shocklayer radiance for a theater missile defense (TMD)-like interceptor. Predictions of the spectral radiance shocklayer for a realistic missile shape will be given. Finally, operations and instrumentation for an upcoming flight designed to test these predictions will then be discussed. The goal of the experiment is to support the development of a two-color detection strategy based on both *short* and long wavelengths to provide a robust onboard seeker environment.

*Research Professor, Department of Chemistry, AIAA senior member.

†Associate Director, Engineering Sciences Division, AIAA Associate Fellow.

‡Technology Agent, AIAA member.

§Technical Program Manager, Center for Space Engineering, AIAA member.

¶Professor, Department of Physical Science, AIAA member

The Operational Context for a Two-Color, MWIR/UV-Visible Seeker

The Ballistic Missile Defense Organization (BMDO) is tasked with providing a missile defense system to protect the U.S., its forces deployed abroad, and its friends and allies against accidental, unauthorized, and limited ballistic missile strikes. The agency has three mission focus areas. The first priority is to develop and deploy increasingly capable Theater Missile Defenses (TMD) to meet existing missile threat to deployed U.S. and allied forces (emerging threats to include cruise missiles). The second priority as a hedge against the emergence of long-range ballistic missile threats, develop options to deploy a National Missile Defense (NMD) for the United States. The third priority is to continue supporting research on more advanced ballistic missile defense technologies to keep pace with the threat and improve the performance of theater and NMD systems.

To realize these goals, one strategy is to impact a warhead with a kinetic kill vehicle (KKV). In pursuit of this end, the KKV has a requirement for sensing and tracking a target candidate, providing the necessary guidance functions in formulating a strategy to collide with a target, and to carry out a vehicle control function in accordance with the guidance plan. A main component of the target acquisition system suite is the optical sensors. When a KKV travels through atmosphere at hypersonic velocities, aerodynamic heat loading causes temperature increases on KKV external surfaces, including optical windows, and thermal excitation of species in the fluid boundary layer and the hyper-shock layer. The consequences of the increase in thermal loading on the optics and fluid temperature increases could potentially be to blind the sensor at specific wavelengths.

The Science and Technology Directorate of the Ballistic Missile Defense Organization is conducting programs to characterize and measure the optical radiation emitted by the flows about hypersonic vehicles.[2] In addition to understanding the basic physics of high temperature plasmas, ongoing analyses are establishing how such emissions are useful for the detection of strategic[3] and theater missile targets.[4] In particular, ultraviolet (UV) radiation offers an attractive potential. UV detector materials have high sensitivity, and detector architectures are mature, generally uncooled, and space qualified. An important application of UV detection is for an onboard seeker, especially where the enhanced spatial resolution is crucial. For such applications, such as boost phase intercept, there is sufficient signal-to-noise for moderate detection ranges.

However, in addition to the above there is another important reason for the use of UV sensors. Generally, a cooled, MWIR sensor is considered as the primary sensor by the community due to its hardware maturity and ample S/N. An important reason to include a second color wavelength is to increase the information content of the detected scene. An operationally relevant image will contain pixels with bright and dim intensities. Target tracking algorithms then have to determine which pixels contain the target, usually based on temperature or brightness. For example, dim pixels may contain the target. The bright pixels could cause confusion because of deliberate countermeasures (CM) such as decoys or natural CMs such as staging events or a plume. This is not a trivial task since the inherent dynamic range for any of these focal planar arrays (FPA) is at best a factor of 500 - 1,000. The concept therefore is to choose a FPA at a second wavelength to provide a discrimination capability. Discrimination is enhanced if the physics of the emission mechanisms is sufficiently different from that of the baseline wavelength. The simplest, cogent argument for the choice of a shorter wavelength, rather than a longer wavelength second color is the blackbody law of radiation. A short and long wavelength combination provides greatest sensitivity to changes in the source brightness.

This paper presents the elements of supporting research required to analyze the key components of a dual-mode interceptor-borne seeker. First the onboard seeker environment is considered. In the next section calculations of the UV and IR shocklayer radiance for a TMD-like interceptor are shown. These calculations present information about the seeker/window background radiation. Since fundamental shocklayer optical spectral radiation data is not available, a sounding rocket flight experiment, called Dual-Mode Experiment on Bowshock Interactions (DEBI), is being planned with an expected launch date of January, 2000.

The goal of the DEBI flight is to develop further understanding of the dynamics inherent with the mission of a KKV in attempt to mitigate operational failure from loss of detection ability. This experiment will fly the same trajectory as the Bow Shock Ultra Violet (BSUV) 1 flight, *i.e.*, achieve a speed of 3.5 km/sec by 40 km altitude, but will emphasize IR spectral measurements. The 4 inch nose radius of the BSUV 1 vehicle will be reduced to a value of less than 2 inches. The calculations shown in this paper use the configuration of the proposed Advanced

Interceptor Technology (AIT) vehicle which has a more slender forebody than that flown in the Bow-Shock flights. The use of an IR spectrometer, never before flown in such a configuration, will provide diagnostics of the shocklayer modeling complementary to our earlier work in the UV.[5, 6]

Shocklayer Flow and Radiance Calculations

The flow calculations were performed with a thermochemical nonequilibrium Navier-Stokes model. The finite-rate chemistry calculations included all of the dry air species (N_2, O_2, NO, N, and O) reactions included in earlier work as well as reactions involving the minor species of H_2O, OH, H, CO_2, C, and CO. The reactions of these species were overlayed with the steady state solution of the dry air species calculations. Table 1 lists the chemical reactions modeled that are additional to the baseline set used to model N_2, O_2, and NO shocklayer species. The rate constants used in the flow modeling are also provided. It should be noted that the thermochemical model includes the key, potential radiators in the IR and UV: NO, NO_2, H_2O, OH, CO_2, and CO.[7]

The two sources of shocklayer radiation are from molecules that are present in the atmosphere and those that are formed in the bow-shock chemistry. Molecules such as CO_2 and H_2O are present in the atmosphere in the trace quantities indicated in Table 2 and used in the calculations.[8, 9] The presence of water, even in trace amounts, in the atmosphere has the effect of also providing additional radiators in the IR and UV spectral regions. Water and OH contribute to the IR spectra and OH is a strong radiator in the ultraviolet.[10] The bow shock chemistry produces NO from the major atmospheric species of N_2 and O_2. The NO radiates both in the IR and the UV.[11]

Figure 1 shows the computational mesh used to represent the AIT-like forebody of the DEBI flight vehicle. The location of the side-view window(s) is also shown since the flight experiment will make observations in this spatial region of the flow. The same computational grid was used for all the solutions presented in this work. The heavy particle translational, vibrational, and rotational temperatures were computed for each solution. Figure 2 shows an enlargement of the stagnation region at 40 km, where the difference in magnitudes and spatial distribution between the translational and vibrational temperatures is most pronounced. The translational temperature reaches a maximum of about 6,000 K as compared with a maximum vibrational temperature of approximately 4,500 K. As expected the translational temperature is much lower in the region of the side-mounted window than at the stagnation point, but still higher than the vibrational temperature. At 50 and 60 km the degree of thermal nonequilibrium increases and the difference in the spatial distribution of the translational and vibrational temperatures is even more pronounced.

Figure 3 shows a comparison of the number density distribution of NO and CO_2 at 40 km altitude in the vicinity of the stagnation region where the spatial variability of the CO_2 species can be seen to be much less than that of NO. Nitric oxide is formed in the stagnation region at a maximum quantity of about 10^{17} number/cm^3, however, at the location further aft the spatial extent of these high number densities is greatly reduced compared to the CO_2 number density. In fact, comparison of the relative NO and CO_2 concentrations at higher altitudes (for the same speed) showed that only at 40 km and in the stagnation region is the NO concentration significantly higher. Figure 4 shows a comparison between the spatial dependence of water and OH about the body. In a manner similar to CO_2, the water has an almost constant distribution about the body. In contrast, the maximum OH concentrations are found to be in the stagnation region where there is the greatest amount of water dissociation. However, the amount of water dissociation is low, thus we would expect a small spectral contribution from OH.

Using the translational temperature and species distributions, the IR spectra were computed using the ATHENA[12] radiative transport band model. A spectral resolution of 25 cm^{-1} was used since that is the anticipated spectral bandwidth of the onboard spectrometer. Spectra that will be shown here correspond to the middle of the side-viewing window region shown in Fig. 1. Figure 5 shows the spectra from 1.5 to 5 μ at 3.5 km/sec, 40 km altitude. Of course the spectrometer will measure the composite spectra, but for the purpose of analyzing the spectra the separate molecular components are shown. It can be seen that the dominant radiator for these conditions is CO_2 and then water, consistent with the flowfield species distributions discussed above.

The calculations of Trolier *et al* [13] suggest that NO_2 could contribute to the spectra in the region between about 3.5 and 4 μ. The figure shows that we predict a small amount of NO_2 radiation and is consistent with our flow chemistry modeling which predicts orders of magnitude less NO_2 concentration than NO. The main production mechanism for NO_2 was found to be the reverse process of the sixth ex-

change reaction given in Table 1.

Although the experiment will not be flown at variable speeds (in a single sounding rocket launch), it is interesting to compare the spectra given in Fig. 5 with that predicted for a flight at 5 km/sec and 40 km altitude. Figure 6 shows the predicted spectra at the higher speed. Consistent with the thermochemical model, the higher speed increases the chemical reaction rates to produce more NO and NO_2. Figure 7 shows the total spectra at an altitude of 30 km for three different speeds. Again, as the collision rates increase (higher speeds) the species that are produced by the shocklayer chemistry contribute more to the spectra. At lower speeds the opposite is seen (see the curve at 2.5 km/sec.) For a fixed speed the shocklayer kinetics will also vary at different altitudes and the NO and NO_2 features will be more evident at lower altitudes.

Radiation calculations were performed in the UV spectral region using the same flow solutions using modifications[10] to the NEQAIR (non-equilibrium air radiation) model of Park.[14] The two main spectral components in the UV are those of the OH and the combined NO (γ, β) and the O_2 Shumann-Runge band systems. The computed spectra were integrated over the filter shapes of two bandpass filters used on previous flights with spectral properties of 230 ± 25 Å(for NO radiation) and 310 ± 5 Å(for OH radiation). Figure 8 shows a predicted signal variation *at the stagnation point* on the order of five orders of magnitude which is typical of the dynamic range of these instruments. The same calculations were also performed in the vicinity of the side-viewing window. It was found that both the NO and OH spectral radiance values were six orders of magnitude below those at the stagnation point.

The calculations point to an important operational result. The shape and window placement of the AIT is such that there is a lack of UV shocklayer radiance for the side window. For a boost phase interceptor viewing a bright UV source, the nonexistent shocklayer radiance coupled with transmissive window materials provides an insurance/alternative to the MWIR sensor. This is particularly significant since the UV is much less affected by interference from hot optical surfaces, such as the window, than the MWIR. The flight measurements will fly instrumentation sensitive enough to verify this important prediction.

Carbon Dioxide Vibrational State Modeling

Examination of the IR calculated shocklayer spectra shown in Figs. 5-7 demonstrates that radiation from shock-heated ambient CO_2 is predicted to be of high importance. The spectra were calculated assuming that the distribution of vibrational states is determined by the flowfield translational temperature. This assumption should be reasonable for conditions where the collision rate is high, especially for a polyatomic system with many possible modes for equilibration. However, as already shown there are portions of the altitude-velocity trajectory parameter space where the flow is not in thermochemical equilibrium. Hence a full vibrational state CO_2 model was developed. Details of the development were given in earlier work,[7] a summary will presented here.

The vibrational state-specific model considers the following types of excitation processes:

$$\begin{aligned}
CO_2(l) + M &\overset{k_{li}}{\longleftrightarrow} CO_2(i) + M, \\
CO_2(l) + N_2(v=0) &\overset{k_{li}^{vv'}}{\longleftrightarrow} CO_2(i) + N_2(v'=1) \\
CO_2(l) + CO_2(v) &\overset{k_{li}^{vv'}}{\longleftrightarrow} CO_2(i) + CO_2(v'), v \neq v'
\end{aligned}$$

where the first process involves $V-T$ collisions with a third body, $M = N_2$, O_2, O, and CO_2, and the last expression represents a $V-V$ process. The rates are taken from the work of Blauer and Nickerson.[15] and Limbaugh and Drakes.[16] The $V-V$ process with N_2 is a near-resonant process and is potentially a major contributor to the excitation of the ν_3 fundamental mode and the combination bands. The ladder of CO_2 vibrational states extends up to energies of 10,000 cm^{-1} (state specific levels are maintained for the $\nu_3 = 1, 2, 3$ fundamental mode up to energy levels of 5,800., 6,200., and 6,700. cm^{-1}, respectively). The inclusion of high energy states provides a reservoir that is necessary to ensure completeness (or, results that are independent of the upper state cutoff). States with the fundamental vibrational mode quantum numbers ν_i for $i = 1, 2, 3$ with maximum values of 4, 8, and 2, respectively are included in the model.

Figure 9 shows the a comparison of the CO_2 vibrational state populations predicted by the state specific model with that of a Boltzmann distribution at the translational temperature. Such comparisons can be made anywhere in the flowfield, at any altitude, but the enormity of the comparisons would make it difficult to visualize. For example at a given altitude there are 100 × 100 (grid points × grid points) such possible comparisons. Instead two locations were chosen that represent the extrema in equilibrium conditions in the flight regime of interest: locations 1 and 2 correspond to a point along

the stagnation streamline at 30 km and a point in the flow near the side mounted window, respectively. Location 1 is a condition close to equilibrium, and the V-V model correctly agrees with a Boltzmann distribution. In contrast, location 2 is a region of the flow where there are fewer collisions, and it can be seen that for the vibrational states responsible for the principal spectral features, their population will be lower than a Boltzmann distribution (note the figure is presented on a log-scale). An important goal of the DEBI flight experiment will be to validate these predictions.

The DEBI Flight Experiment

The DEBI experiment duration is estimated to be approximately forty seconds out of a total vehicle flight time of approximately 800 s. The experiment begins with the launch from NASA Wallops Island Flight Facility (NASA/WFF). The experimental vehicle design reference requirement is to reach an altitude of 40 km with upward velocity of 3.5 km/s. In-flight data is to be acquired above 40 km altitude. A Terrier-Malemute launch vehicle with MK-12 Terrier motor was determined by NASA site engineers to provide sufficient thrust levels for a payload weight of about 200 lbs. to meet the ascent requirements. See Ref. 17 for more details. Figure 10 depicts the typical mission operations for the DEBI flight on the NASA/WFF range. Note that the science mission is predicted to be concluded within approximately forty seconds into flight.

The payload elements, designed and fabricated by SDL, include structures, thermal control, power, telemetry, command and data handling, and payload fairing. SDL is chartered with building the payload component such that the sensors survive the flight environment and satisfy science requirements until the end of the defined experiment. The payload component has three interfaces: the Malemute interface, the sensor packages interface, and interfaces with the ground segment.

An important operational component of missile design if the use of a protective fairing for sensor protection during the early portion of the missile flyout where heating rates are prohibitively high. As part of DEBI flight experiment a fairing is used to protect the viewport windows until approximately 40 km, where the dynamic pressure and heating rates for sensor windows are sufficiently reduced. Figure 11 shows the payload fairing assembly which is designed to deploy at 40 km altitude. Ground testing was conducted on a spin table at Space Dynamics Laboratory to ensure that the separation dynamics are well understood. A timer circuit that activates a pyrotechnic cable cutter initiates payload fairing separation. A combination of spring and centripetal forces cause the payload fairing to jettison away from the DEBI payload without hitting the Malemute stage. During mission operations significant optical measurements are expected to appear in the telemetry bit stream at the instant of payload fairing separation.

The sensor packages consist of detectors connected via fiber optic bundles to apertures positioned at the vehicle stagnation point and two symmetrically aft-stationed points downstream of the vehicle nose. The data to be acquired are collected from 16 spectrometer channels, 8 mid wave infrared (MWIR) channels, 6 mid-wave short wave infrared (SWIR) channels, 2 UV channels and an array of temperature sensors. Table 3 provides a summary of the key instrument characteristics.

Figure 12 shows a schematic of the payload forebody showing the view locations and fiber-optic implementation. The nose cone tip for the vehicle (also shown in the figure) was designed by engineers at the Space Dynamics Laboratory (SDL), at Utah State University. The stagnation point at the nose cone tip is fitted with a recessed sapphire lens connected to a fiber optic bundle. Is should be noted that the section at the very tip of the nose section is specified copper to help meet thermal stability requirements.

The UV detectors provide legacy data overlap with the BSUV I and II experimental flights. One feature of the DEBI UV sensors is that they are designed to measure very low intensities in the side viewing directions where it is anticipated that the signal levels will be quite low.

The MWIR and SWIR radiometers have InGaAs and HgCdTe photodiode detectors coupled to windows with IR Fluoride glass fibers. The scanning infrared (IR) spectrometer has fast a f/0.5 relay lens system at the exit slit and a stepper motor driven diffraction grating with InGaAs photodiode detectors for the short wavelength regions, extended InGaAs photodiode detectors for the intermediate wavelength regions, and photo-voltaic short wavelength HgCdTe for the longest wavelength regions. All detectors will be cooled below 193K (-80C) before flight. Since the time of flight is so short (40 seconds) the thermal inertia of the vehicle is sufficient to preclude the complication of in-flight cooling.

Conclusions

This paper has presented a methodology for the

calculation of the self-induced, shocklayer radiance for a theater missile defense (TMD)-like interceptor. Predictions of the shocklayer spectral radiance for a realistic missile shape show that there is a "window" in the shocklayer radiance between 3.5 to 4 μ and in the UV. Operations and instrumentation for a low cost, relatively simple, upcoming flight designed to test these predictions and verify whether this window exists for an operational system such as AIT have been presented.

Examination of Fig. 8 shows that a compelling argument can be made for the use of a dual-mode seeker for a boost phase interceptor. The predicted UV radiation in front of a side mounted window on a slender body is non-existent. The high temperature spectral features of UV-transmissive windows such as sapphire and quartz remain high at typical interceptor window temperatures, *without window cooling*. Hence, the use of a second wavelength in the UV provides a good insurance policy against opaque, non-transmissive window optics in the MWIR. The goal of the upcoming experiment is to support the development of a two-color detection strategy based on both *short* and long wavelengths and address many of interceptor-sensor operational issues.

Acknowledgments

The work at George Washington University was supported by the Army Research Office Grant DAAG55-98-1-009 under the Ballistic Missile Defense Organization Science and Technology Directorate.

References

[1] D. Levin, L. Caveny, and G. Beaghler, "Dual-Mode Spectral Detection of Hypersonic Flows," Invited paper presented at the *10th Meeting of Optical Engineering in Israel*, March 1997, SPIE.

[2] D. Levin, L. Caveny, D. Mann, and D. Burt, Skipper - An Innovative US and Russian University Space Science Mission, presented at the SPIE OE/Aerospace Sensing Meeting, 4-6 April 1994, Orlando, FL. Published with the SPIE Proceedings of Aerial Surveillance Sensing Including Obscured and Underground Object Detection, Vol. 2217, pp. 292-306.

[3] D. Levin, R. Collins, G. Candler, "The Utility of Ultraviolet Bow Shock Radiation to Terminal Interceptor Systems," IDA Paper P-2697, April 1992.

[4] D. Levin, R. Collins, L. Caveny, D. Tietz, and D. Mann, "The Measurement and Application of Aerodynamically Induced Optical Signature Ultraviolet," Invited paper presented at the 8th Meeting of Optical Engineering in Israel, December 1992.

[5] P. W. Erdman, E. C. Zipf, P. Espy, C. Howlett, D. A. Levin, R. Loda, R. J. Collins, and G. V. Candler, "Flight Measurements of Low Velocity Bow Shock Ultraviolet Radiation," *Journal of Thermophysics and Heat Transfer*, **7**, 37 (1993).

[6] D. A. Levin, G. V. Candler, R. J. Collins, P. W. Erdman, E. Zipf, P. Espy, and C. Howlett, "Comparison of Theory with Experiment for the Bow Shock Ultraviolet Rocket Flight," *Journal of Thermophysics and Heat Transfer*, **7**, 30 (1993).

[7] Levin, D., Candler, G., and Limbaugh, C., "Multi-spectral Shocklayer Radiance from a Hypersonic Slender Body," *AIAA Paper No. 99-3747*, 33rd Thermophysics Conference, Norfolk, VA.

[8] Jurda, A. S., Handbook of Geophysics and the Space Environment, United States Air Force, 1985.

[9] Brasseur, G. and Solomon, S., Aeronomy of the Middle Atmosphere, D. Reidel Publishing Company, Second Edition.

[10] Levin, D., Collins, R., Candler, G., Wright, M., and Erdman, P., Examination of OH ultraviolet radiation from shock-heated air, *Journal of Thermophysics and Heat Transfer*, 1996, 10: 200.

[11] P. W. Erdman, E. C. Zipf, P. Espy, C. Howlett, D. Levin, R. Collins, and G. Candler, "Measurements of Ultraviolet Radiation from a 5 km/sec Bow Shock," *Journal of Thermophysics and Heat Transfer*, **8**, 441 (1994).

[12] Devore, John G., "ATHENA User's Guide", PRI Technical Memo, September 1987.

[13] J. Trolier, D. Hudson, D. Carlson, and W. Krawczyk, "Shocklayer Radiance Effects on Endoatmospheric Interceptor Seeker Performance," *AIAA Paper No. 92-2816*, May 19, 1992.

[14] Park, C., "Calculation of Nonequilibrium Radiation in the Flight Regimes of Aero-Assisted Orbital Transfer Vehicles," *Thermal Design of Aero-Assisted Orbital Transfer Vehicles*, Ed. H. F. Nelson, Progress in Astronautics and Aeronautics, **96**, 1985.

[15] Blauer, J. A. and Nickerson, G. R., "A Survey of Vibrational Relaxation Rate Data for Processes Important to CO_2-N_2-H_2O Infrared Plume Radiation," AFRPL-TR-73-57, October 1973.

[16] Limbaugh, C. C., and Drakes, J. A., "CO_2 vibrational relaxation effects in a laser-heated hypersonic flow," *AIAA Paper No. 97-2492*, 32nd Thermophysics Conference, June 23, 1997, Atlanta, Ga.

[17] Sounding Rocket User's Handbook, NASA/GFSC/WFF, September 1998.

Table 1: Thermochemical Model and Rate Coefficients[a]

Reaction	C_{fi}[b]	η_i	E_{fi}/R[c]	Third Body, M
Dissociation:				
$H_2O + M \rightarrow OH + H + M$	3.5 x 10^{13}	0.0	50,584	N_2
$OH + M \rightarrow O + H + M$	7.5 x 10^{11}	0.06	50,563	N_2
$CO_2 + M \rightarrow CO + O + M$	6.9 x 10^{18}	-1.5	63,275	N_2, O_2, NO
	1.4 x 10^{19}	-1.5	63,275	N, O
$CO + M \rightarrow C + O + M$	2.3 x 10^{17}	-1.	129,000	N_2, O_2, NO
	3.4 x 10^{17}	-1.	129,000	N, O
Exchange:				
$O_2 + H \rightarrow O + OH$	2.2 x 10^{11}	0.0	8,377.5	
$H_2O + O \rightarrow 2OH$	6.8 x 10^{10}	0.0	3,492.7	
$CO + O \rightarrow O_2 + C$	3.9 x 10^{10}	-0.18	69,200	
$CO_2 + O \rightarrow O_2 + CO$	2.1 x 10^{10}	0.0	27,800	
$N + NO_2 \rightarrow 2NO$	2.41 x 10^{9}	0.0	-500	
$NO_2 + O \rightarrow NO + O_2$	1.02 x 10^{10}	0.0	-300	
Recombination:				
$NO + O + O_2 \rightarrow NO_2 + O_2$	1.45 x 10^{9}	0.0	900	
$NO + O + N_2 \rightarrow NO_2 + N_2$	2.03 x 10^{9}	0.0	900	
$2NO + O_2 \rightarrow 2NO_2$	1.2 x 10^{3}	0.0	530	

[a]Rate coefficient is $C_{fi}T_i^{\eta}\exp(-E_{fi}/T)$

[b]Rates are in cm^3/mole-sec or higher.

[c]$R = 1.98$ cal/mole-K, E_{fi} is in cal.

Table 2: Atmospheric Conditions

Altitude (km)	Number Density (number/cm^3)	Water Mixing Ratio	CO_2 Mixing Ratio
40	8.26e16	1.6e-5	3.4e-4
50	2.19e16	1.6e-5	3.4e-4
60	6.67e15	1.5e-5	3.4e-4

Table 3: Instrument Characteristics and Locations on DEBI Flight Vehicle.

	Fiber Location at Aperture	Instrument	Spectral Features	Comments
1	stagnation point	UV photo-multiplier	0.24 $\pm$0.04μ	CsTe PMT[a]
2	side station	UV photo-multiplier	0.24 $\pm$0.05μ	CsTe PMT
3 - 8	Side station	MWIR MOM[b] Radiometer with $\sim 0.2\mu$ filter	3.0 - 4.0 μ with 0.2 μ increments	
9	Side station	MWIR MOM Radiometer	3.5 $\pm \sim 0.4\mu$ filter	
10	Side station	MWIR MOM Radiometer	4.3 $\pm \sim 0.1\mu$ filter	tuned for CO_2
11	Side station	SWIR MOM Radiometer	1.0 μ	
12	Side station	SWIR MOM Radiometer	1.27 μ	tuned for O_2
13	Side station	SWIR MOM Radiometer	1.5 μ	tuned for OH
14	Side station	SWIR MOM Radiometer	2.0 μ	tuned for CO_2
15	Side station	SWIR MOM Radiometer	2.3 μ	tuned for predicted "spectral window"
16	Side station	SWIR MOM Radiometer	2.7 μ	tuned for CO_2 and NO
17 - 24	stagnation point	Scanning IR spectrometer	1.0 - 3.0 μ in $\pm 500\mu$ steps	Spectral averaging of 5, 100 Åincrements
25 - 32	side station	Scanning IR spectrometer	1.0 - 3.0 μ in $\pm 500\mu$ steps	Spectral averaging of 5, 100 Åincrements
33 - N	TBD	Temperature	N/A	Resistive temperature elements

[a]PMT - photo-multiplier tube photo-cathode detectors operated in photon counting mode
[b]MOM - Micro Optic Multispectral

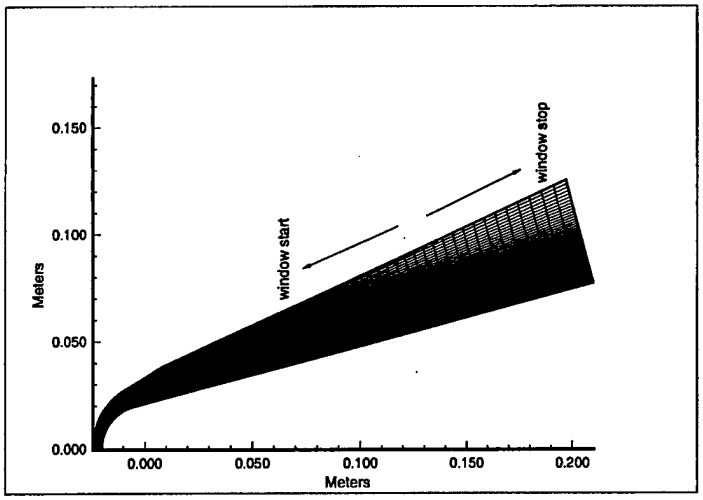

Figure 1: Computational mesh of AIT vehicle.

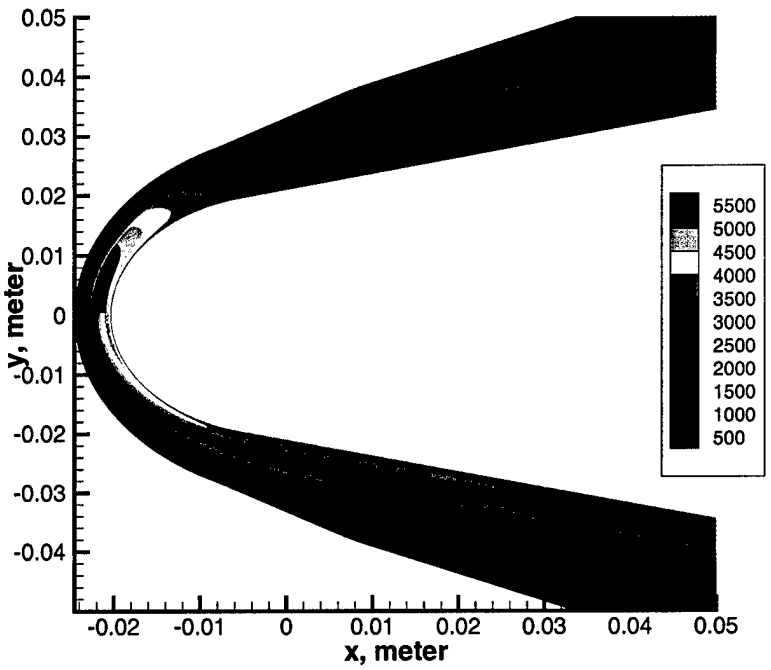

Figure 2: Comparison of translational temperature contours (top) with vibrational temperature contours (bottom) at 40 km altitude, 3.5 km/sec in the stagnation region. Note axes are scaled independently.

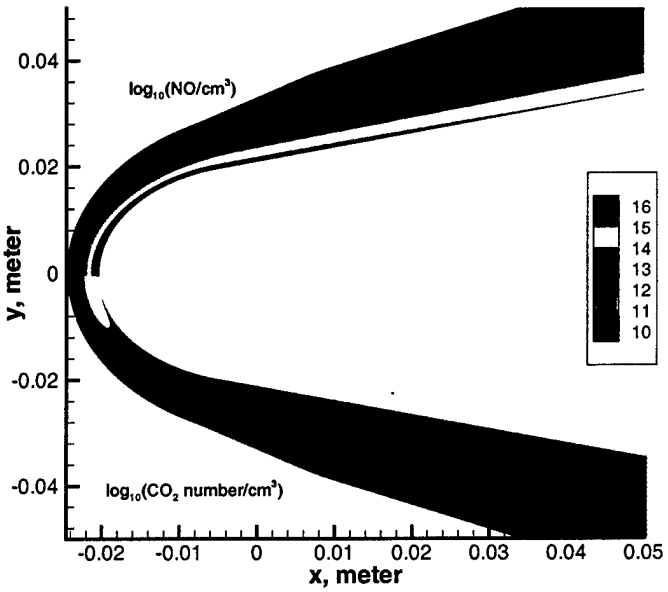

Figure 3: Comparison of number density contours of NO (top) with CO_2 (bottom) at 40 km altitude, 3.5 km/sec in the stagnation region. Note axes are scaled independently.

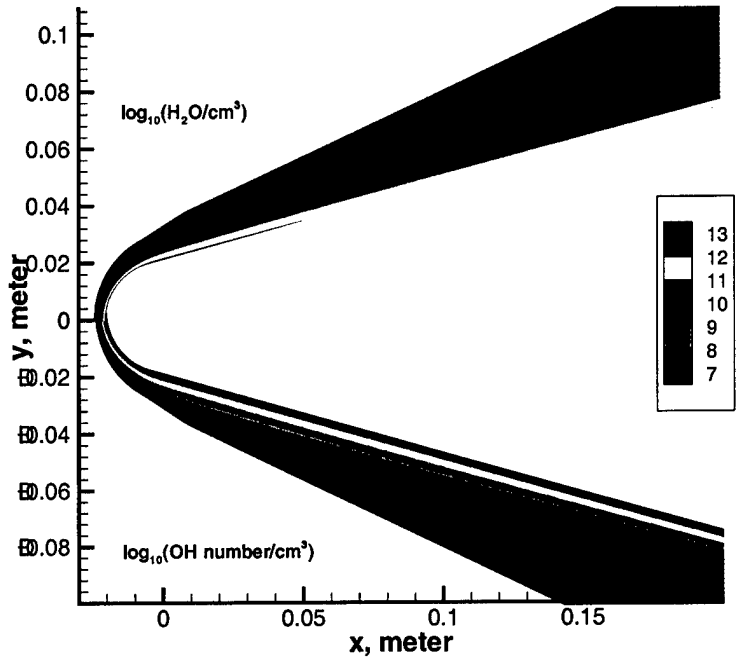

Figure 4: Comparison of number density contours of water (top) with OH (bottom) at 40 km altitude, 3.5 km/sec.

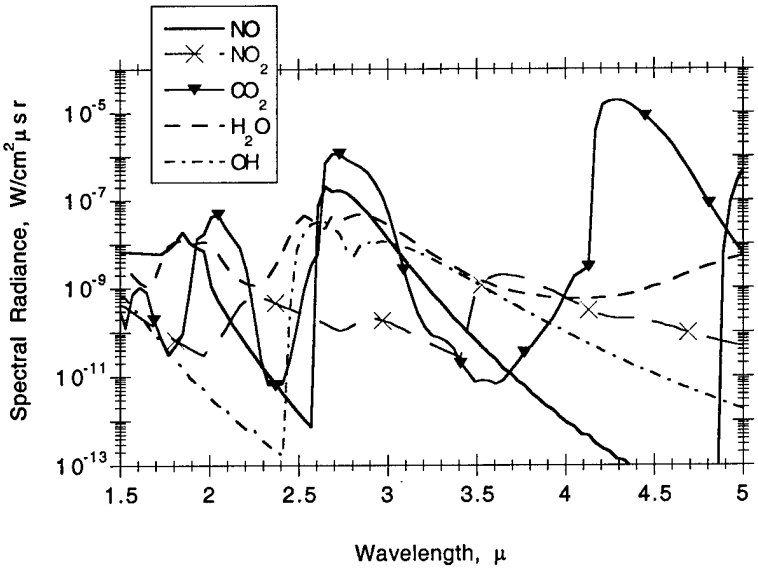

Figure 5: Calculated spectra at 40 km altitude, 3.5 km/sec.

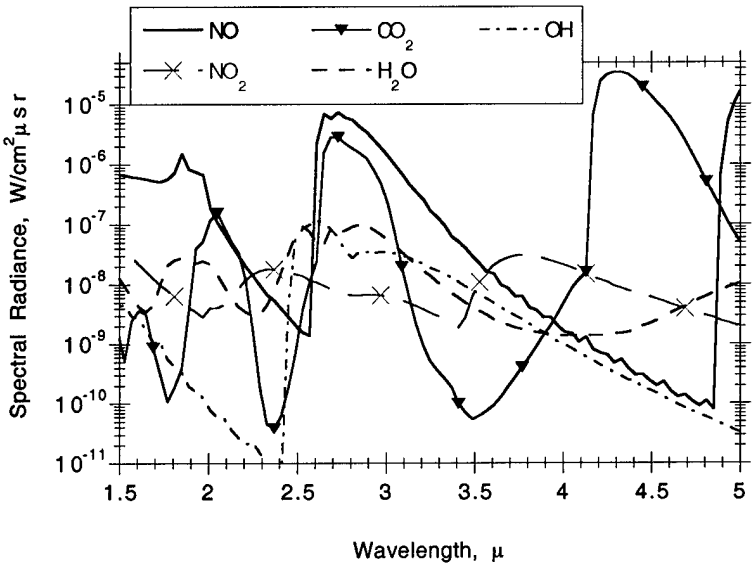

Figure 6: Calculated spectra at 40 km altitude, 5.0 km/sec.

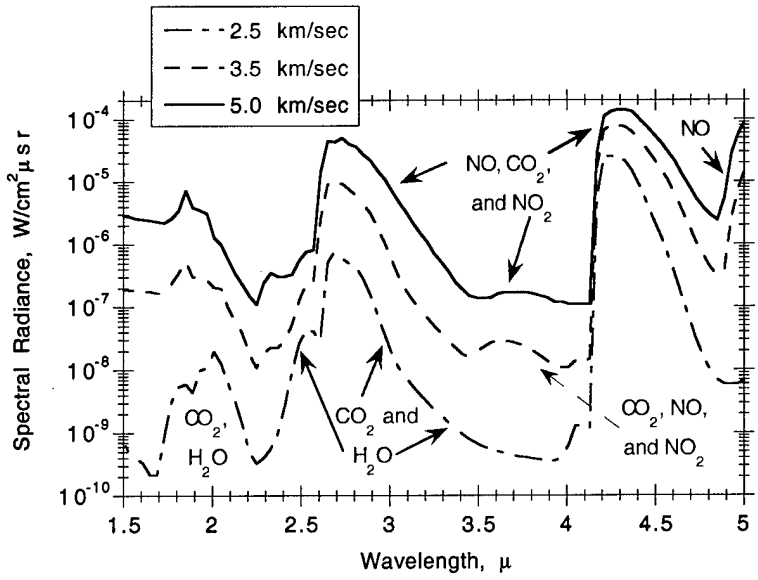

Figure 7: Comparison of calculated spectra at 30 km altitude for different speeds.

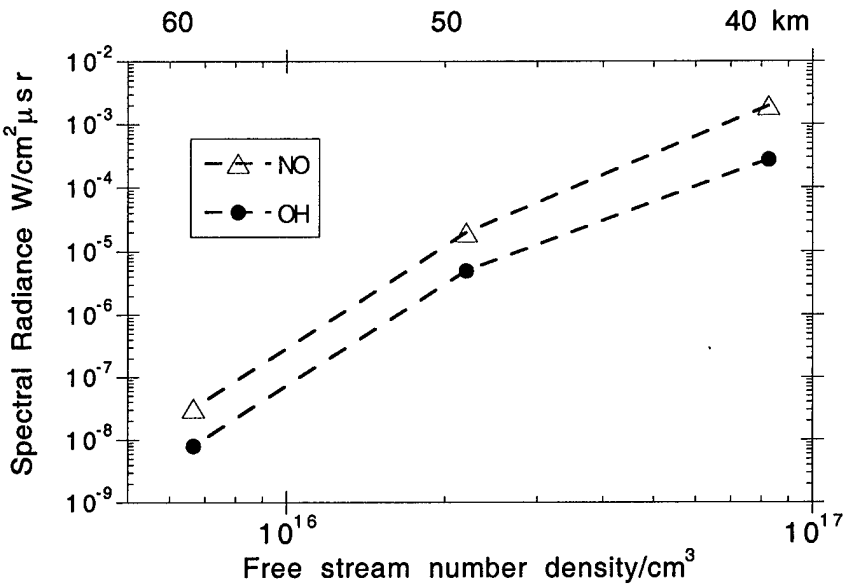

Figure 8: Altitude dependence of stagnation viewing UV photometers.

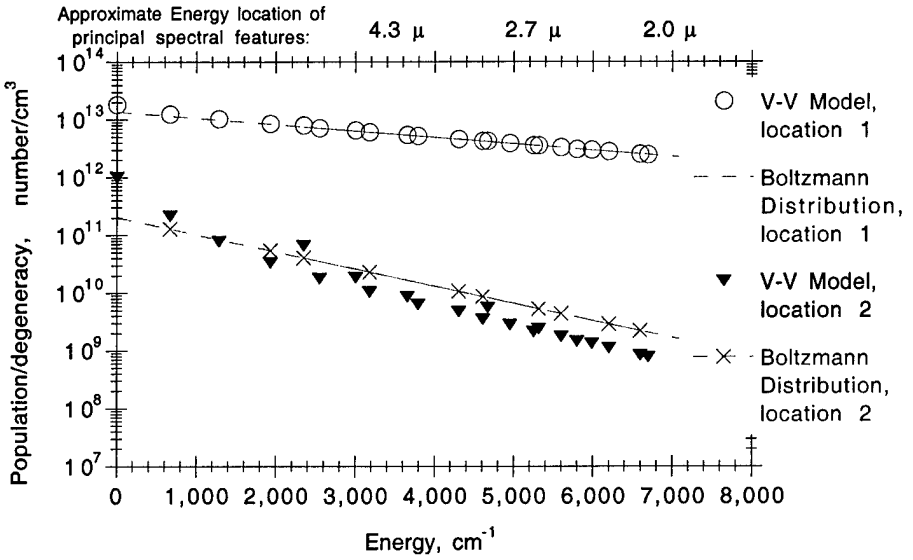

Figure 9: Comparison of predicted CO2 vibrational populations with a Boltzmann distribution at 3.5 km/sec for two locations in the flow. (see text)

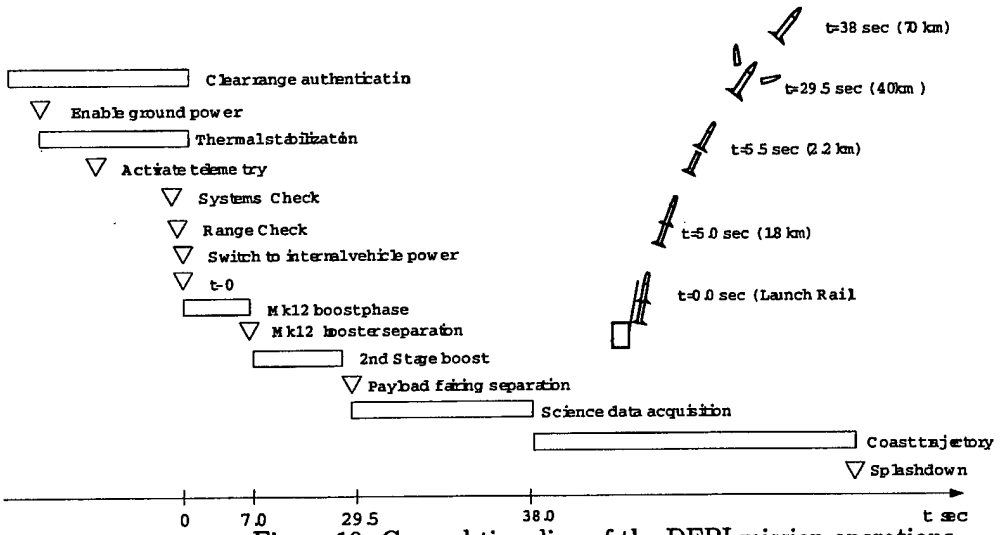

Figure 10: General time-line of the DEBI mission operations.

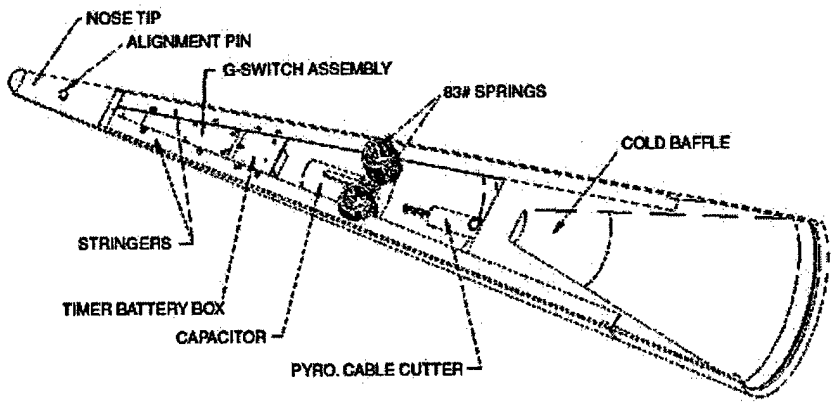

Figure 11: Oblique view of the payload fairing half jettisoned at 40 km altitude (source SDL).

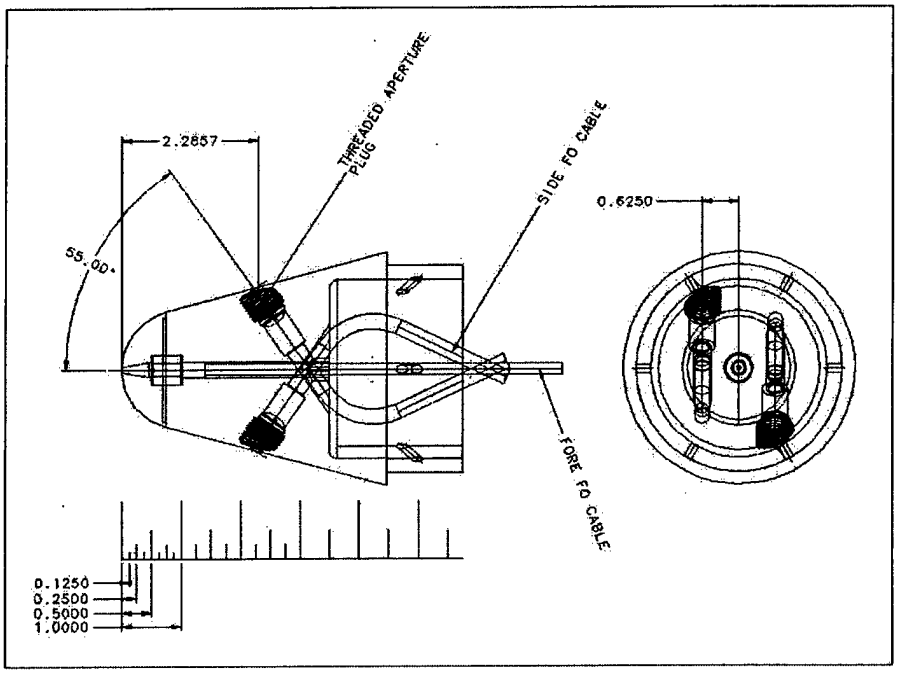

Figure 12: Nose cone design for the DEBI flight and instrument layout.